

An Interactive Shader for Natural Diffraction Gratings

Bachelorarbeit

der Philosophisch-naturwissenschaftlichen Fakultät
der Universität Bern

vorgelegt von

Michael Single

2014

Leiter der Arbeit:
Prof. Dr. Matthias Zwicker
Institut für Informatik und angewandte Mathematik

Abstract

In nature color production is the result of physical interaction of light with a surface's nanostructure. In his pioneering work, Stam developed limited reflection models based on wave optics, capturing the effect of diffraction on very regular surface structures. We propose an adaption of his BRDF model such that it can handle complex natural gratings. On top of this, we describe a technique for interactively rendering diffraction effects, as a result of physical interaction of light with biological nanostructures such as snake skins. As input data, our method uses discrete height fields of natural gratings acquired by using atomic force microscopy (AFM). Based on Taylor Series approximation we leverages precomputation to achieve interactive rendering performance (about 5-15 fps). We demonstrate results of our approach using surface nanostructures of different snake species applied on a measured snake geometry. Lastly, we evaluate the qualty of our method by a comparision of the maxima for peak viewing angles using the data produced by our method against the maxima resulting by the grating equation.

Contents

1 Evaluation and Data Acquisition	1
1.1 Data Acquisition	1
1.2 Diffraction Gratings	1
1.3 Verifications	7
1.3.1 Numerical Comparisons	8
1.3.2 Virtual Testbench	9
2 Results	12
2.1 BRDF maps	12
2.2 Snake surface geometries	21
List of Tables	27
List of Figures	27
List of Algorithms	28
Bibliography	29

Chapter 1

Evaluation and Data Acquisition

1.1 Data Acquisition

Our goal is to perform physically accurate simulations of diffraction effects due to natural gratings. As for every simulation, its outcome highly depends on the input data and thus we also require measurements¹ of real natural gratings. For that purpose, samples of skin sheds of Xenopeltis and Elaphe snake species were fixed on a glass plate and then, by using an Atomic Force Microscope (AFM), their surface topography was measured and stored as grayscale images, indicating the depth. In general, an AFM is a microscope that uses a tiny probe mounted on a cantilever to scan the surface of an object. The probe is extremely close to the surface, but does not touch it. As the probe traverses the surface, attractive and repulsive forces arising between it and the atoms on the surface induce forces on the probe that bend the cantilever. The amount of bending is measured and recorded, providing a depth-map of the atoms on the surface. An Atomic force microscope is a very high-resolution probe scannings, with demonstrated resolution on the order of a fraction of a nanometer, which is more than 1000 times better than the optical diffraction limit.

1.2 Diffraction Gratings

In order to evaluate the quality of our simulations, it is important to understand what a diffraction grating actually is. An idealised diffraction grating like in figure 1.2 is made of a large number of parallel, evenly spaced slits in an opaque medium. In general, if the spacing between slits is wider than the wavelength of the incoming light, then the better we can observe how the light is diffracted on the grating. Simply speaking, each slit in the grating acts as a point light source from which light spreads and propagates in all directions. According to Huygen's Principle the outgoing light may have a different outgoing angle as it had initially. Figure 1.1 illustrates this behaviour for a monochromatic light source passing through a grating and shows that the the outgoing angle will be different from the incident angle. Hence, the diffracted light is composed of the sum of interfering wave components emanating from each slit in the grating.

¹All measured data has been provided by the Laboratory of Artificial and Natural Evolution at Genava - Website:www.lanevol.org

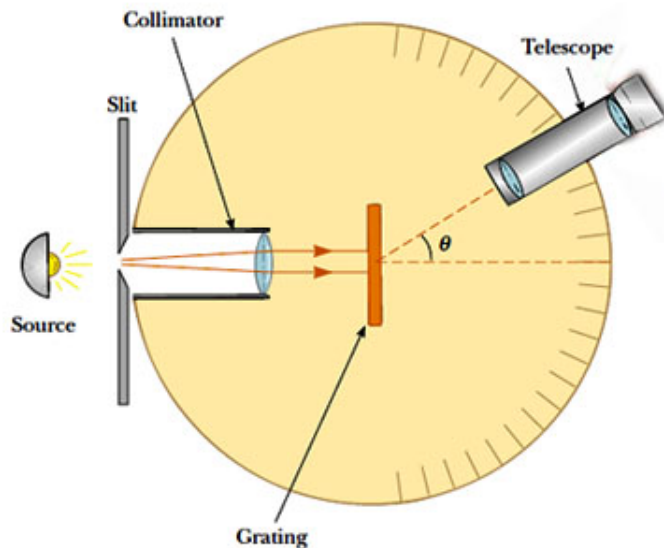


Figure 1.1: Spectrometer: When a beam of monochromatic light passes through a grating placed in a spectrometer, images of the sources can be seen through the telescope at different angles.

Suppose that a monochromatic light source is directed at the grating, parallel to its axis as shown in figure 1.1. Let the distance between successive slits be equal the value d .

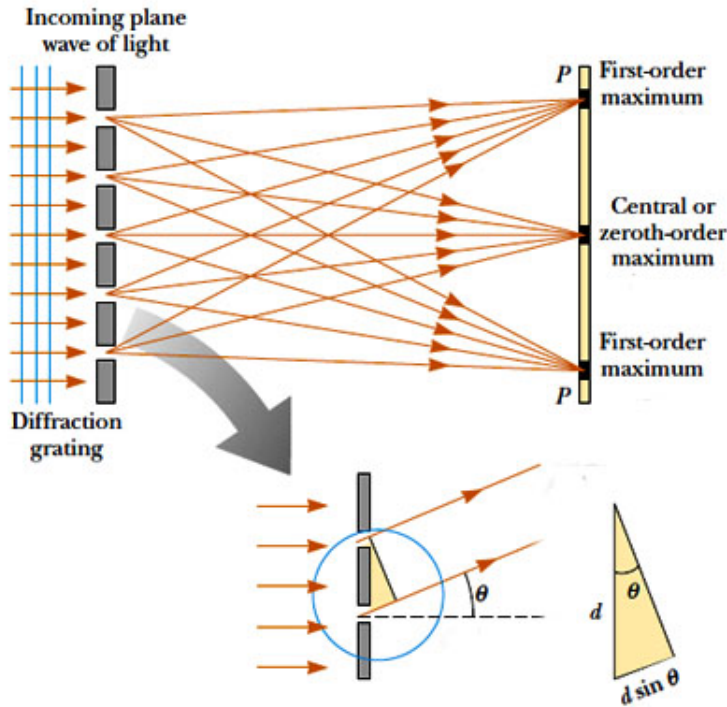


Figure 1.2: Light directed parallel to grating:

The observable diffraction pattern is the result of interference effects among outgoing wavelets according to Huygen's Principle. The path difference between waves from any two adjacent slits can be derived by drawing a perpendicular line between the parallel waves. Applying some trigonometry, this path difference is $d \sin(\theta)$. If the path difference equals one wavelength or a multiple of the wave's wavelength, the emerging, reflected waves from all slits will be in phase and a bright line will be observed at that point. Therefore, the condition for maxima in the interference pattern at the angle θ is:

$$d \sin(\theta) = m\lambda \quad (1.1)$$

where $m \in \mathbb{N}_0$ is the order of diffraction. Because d is very small for a diffraction grating, a beam of monochromatic light passing through a diffraction grating is split into very narrow bright fringes at large angles θ .

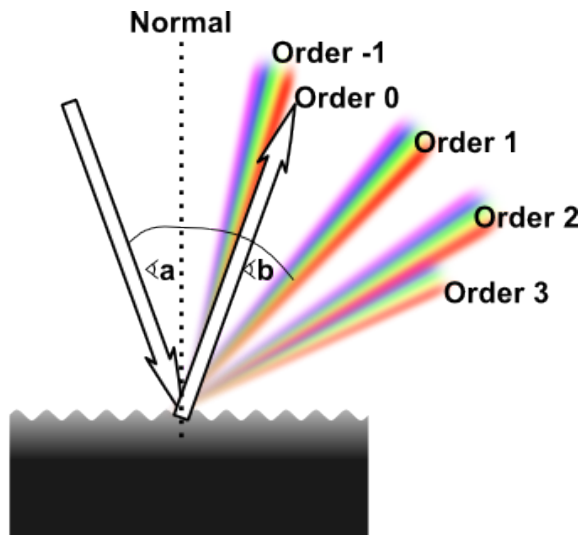


Figure 1.3: Different Orders of diffraction

When a narrow beam of white light is directed at a diffraction grating along its axis, instead of a monochromatic bright fringe, a set of colored spectra are observed on both sides of the central white band as shown in figure 1.3.

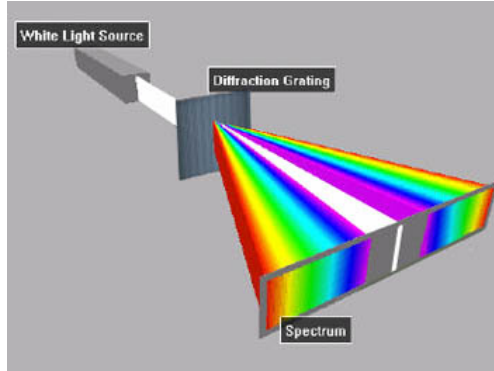


Figure 1.4: White Light beam causes coloured diffraction spectra

Since the angle θ increases with wavelength λ , red light, which has the longest wavelength, is diffracted through the largest angle. Similarly violet light has the shortest wavelength and is therefore diffracted the least. This relationship between angle and wavelength is illustrated in figure 1.4. Thus, white light is split into its component colors from violet to red light. The spectrum is repeated in the different orders of diffraction, emphasizing certain colors differently, depending on their order of diffraction like shown in figure 1.3. Note that only the zero order spectrum is pure white. Figure 1.5 shows the relative intensity resulting when a beam of light hits a diffraction grating for different number of periods. From the graph we recognise that the more slits a grating has, the sharper more slopes the function of intensity gets. This is similar like saying that, the more periods a grating has, the sharper the diffracted color spectrum gets like shown in figure 1.6.

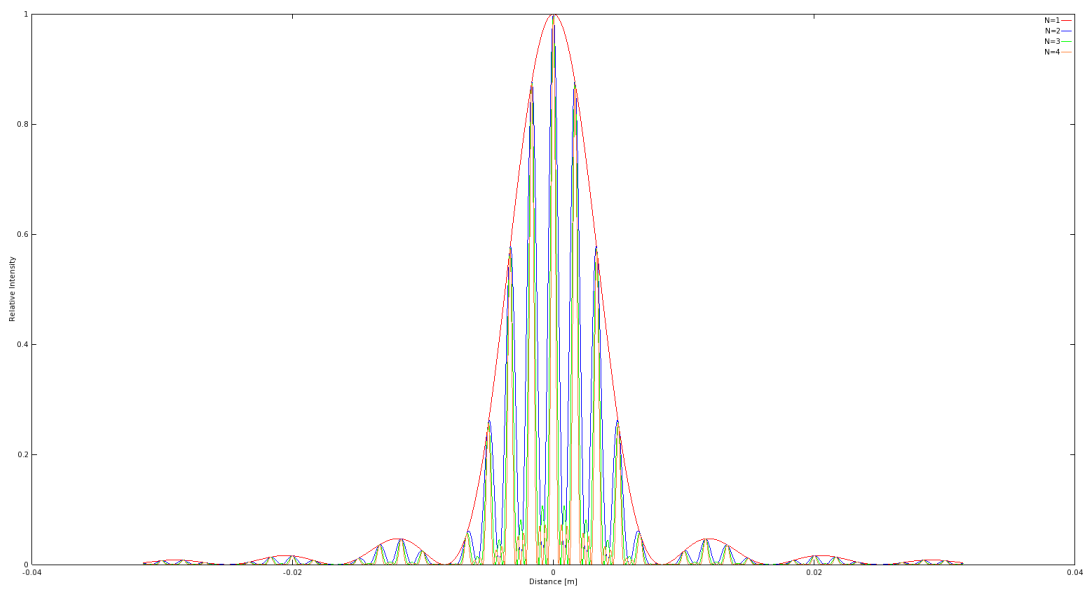
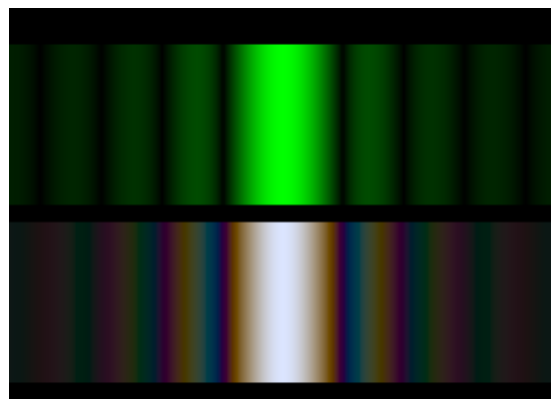
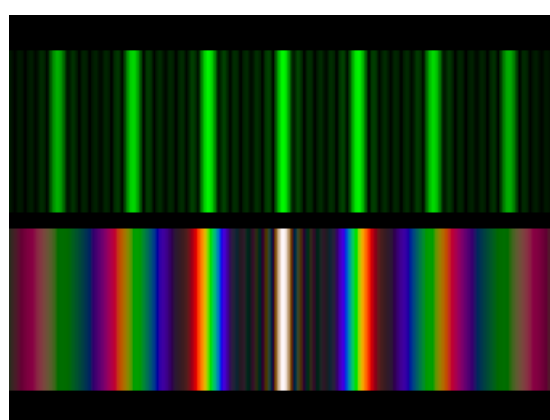


Figure 1.5: Relative intensities of a diffracted beam of light at wavelength $\lambda = 500\text{nm}$ on a grating for different number of periods N width slit width of 30 microns and slit separation of 0.15 mm each. The viewer is 0.5m apart from the grating.



(a) one slit



(b) seven slits

Figure 1.6: Difference of diffraction pattern between a monochromatic (top) and a white (bottom) light spectra for different number of slits.

1.3 Verifications

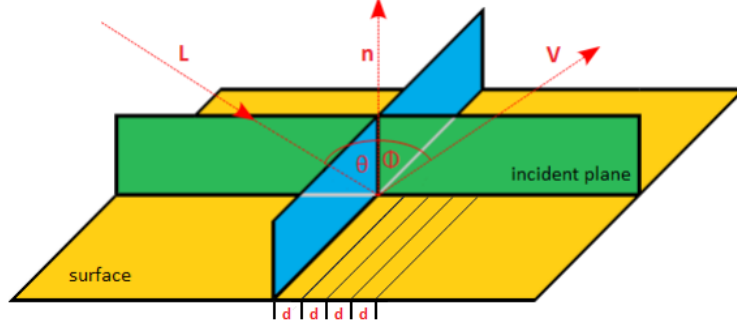


Figure 1.7: Experimental setup for evaluation: A light beam with direction L hits the surface, representing a grating pattern with periodicity d , at the incident plane relative to the surface normal n at angle θ and emerges at angle ϕ with direction V .

The physical reliability of our BRDF models has been verified by applying those on various patches which are a synthetic blazed grating, an Elaphe and a Xenopeltis snake shed sample patch. We compared the resulting response against the response resulting by the grating equation, which models the relationship between the grating spacing and the angles of the incident and diffracted beams of light. Figure 1.7 illustrates the geometrical setup for our evaluation approach: A monochromatic beam of light with wavelength λ hits a surface with periodicity d at an angle θ relative to the normal n along its incident plane. The beam emerges from the surface at the angle ϕ .

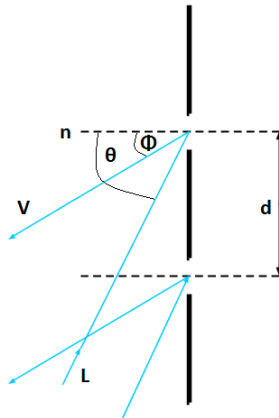


Figure 1.8: Reflecting grating: When the incident light direction is not parallel to its axis at the grating, there is another $\sin(\phi)$ involved. See also the grating equation 1.2.

The maximum in intensity is given by the grating equation derived from the equation 1.1 following figure 1.8:

$$\sin(\theta) = \sin(\phi) + \frac{m\lambda}{d} \quad (1.2)$$

In our evaluation we are interested in the first order diffraction, i.e. m equals one which. We further assume that the incident light direction ω_i is given. In contrast the direction of the reflected wave ω_r is not given. In Mathematics, a three dimensional direction vector is fully defined by two two angles, i.e. it can be represented by spherical coordinates with radius $r = 1$. By convention, we denote those two vectors by θ and ϕ like in figure 1.7. Hence, θ_i , ϕ_i and ϕ_r are given constants whereas θ_i is a free parameter for our evaluation simulation. Therefore, we are going to compare the maxima for peak viewing angles corresponding to each wavelength using data produced by our method against the maxima resulting by the grating equation 1.2.

1.3.1 Numerical Comparisons

For evaluation purposes we have implemented our BRDF models in java. We once again use our geometrical setup as illustrated in figure ?? where θ_i , ϕ_i and ϕ_r are provided as input values and θ_i is a free parameter. Within our evaluation we have set them to $\theta_i = 75^\circ$ $\phi_i = 0^\circ$ $\phi_r = 180^\circ$ degrees. The wavelength space Λ and the range Θ of our free parameter θ_i are discretized in equidistant steps whereas their step sizes are given as input arguments for our Java program:

$$\Lambda = \{\lambda | \lambda = \lambda_{min} + k \cdot \lambda_{step}, \quad k \in \{0, \dots, C - 1\}\} \quad (1.3)$$

where $\lambda_{step} = \frac{\lambda_{max} - \lambda_{min}}{C-1}$ and C is the discretisation level of the lambda space. We similarly discretise the angle space by predefining an minimal and maximal angle boundary and $\text{ceil}(\text{angMax} - \text{angMin})/\text{angInc}$ is the number of angles. Our Java BRDF model implementations are applied on the grid $[\Lambda, \Theta]$ and will store their spectral response in a matrix

$$R = \{\text{response}(\lambda_i, \theta_r^j) | i \in \text{Index}(\Lambda), \quad j \in \text{Index}(\Theta)\} \quad (1.4)$$

We will plot this matrix and compare its graph against the grating equation for similar condition like in stated in algorithm 1.

Algorithm 1 Vertex diffraction shader

```

load matrix R 1.4
λcount = |Λ|
λinc = λmax - λmin
λ = λmin + λinc · (-1 + [1 : λcount])
[maxCmaxI] = max(R)
viewAngForMax = angMin + angInc · (maxI - 1)
thetaV = asin(λ / d - sin(θiπ / 180)) · 180 / π
plot(λ, viewAngForMax)                                ▷ graph resulting by our brdf model
plot(lambda, thetaV)                                  ▷ graph resulting by grating equation

```

1.3.2 Virtual Testbench

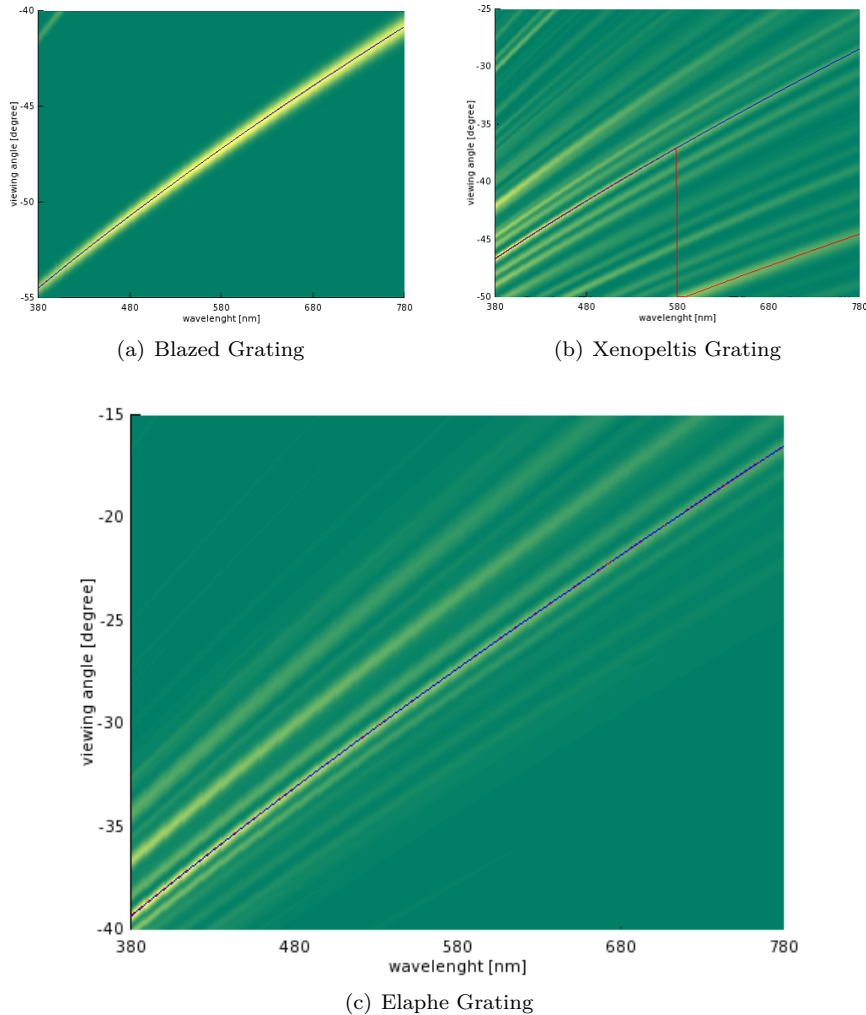


Figure 1.9: Reflectance obtained by using the shading approach described in algorithm ?? simulating a BRDF which models the effect of diffraction at different viewing angles over the spectrum of visible light.

In this section we discuss the quality of our BRDF models applied to different surface structures. For that purpose we compare the resulting relative reflectance computed as described in section 1.3.1 for each of our BRDF models to the idealized grating equation 1.2.

Patch	Mean[mm]	Variance[mm]
Blazed grating 2.2(a)	2500.34	0.16
Elaphe grating 2.2(b)	1144.28	0.15
Xenopeltis grating 2.2(c)	1552.27	0.45

Table 1.1: Statistics of periodicity d of our used gratings 2.2 estimated by using the grating equation 1.2. This table was provided by Mr. D.Singh.

Figure 1.9 shows the reflectance graphs resulting by the shading approach of sampling the whole lambda space described in algorithm ???. This evaluation has been applied to different idealized periodic structures, namely to the Blaze- 1.9(a), Elaphe- 1.9(c) and Xenopeltis grating 1.9(b), using an illumination angle $\theta_i = 75$ degrees. Note that higher response values are plotted in yellow and lower values in green. For each of the graphs we determine the viewing angles with peak reflectance for various wavelengths and then plot this peak viewing angles against their wavelength as solid red curves. The blue curve represents diffraction angles for an idealized periodic structure with a certain periodicity d according to the grating equation 1.2. The corresponding periodicity for every grating structure is estimated using the precomputed response data using again the grating equation and are tabulated in table 1.1.

The red and blue curve are closely overlapping in our figures 1.9(a) and 1.9(c). For Blaze and Elaphe there is only diffraction along only one direction perceivable. Since the Blazed grating is synthetic we use its exact periodicity to plot the blue curve instead of estimating it. The Xenopeltis grating is evaluated just along the direction for the finger like structures. For Xenopeltis it is interesting to see that the red curve for the peak viewing angle toggles between two ridges corresponding to two different periodicities. this happens because there are multiple sub regions of the nanostructure with slightly different orientations and periodicity. Each sub region carves out a different yellowish ridge. depending on the viewing angle, reflectance due to one such subregion can be higher than from the others.

Figure 1.10 shows the evaluation plots for the (N_{min}, N_{max}) shading approach which integrates over a reduced wavelength spectrum applied to the Blaze- 1.10(b) and the Elaphe-grating 1.10(b). This optimization approach is mentioned within the discussion section of the implementation chapter ?? as a run-time complexity enhancement of the whole lambda space sampling approach 1.9. The response curve again closely matches the corresponding grating equation curve for both evaluation graphs and also look similar to the corresponding evaluation plots when integrating over the whole lambda space shown previously in figure . Therefore we may assume this optimization to be valid.

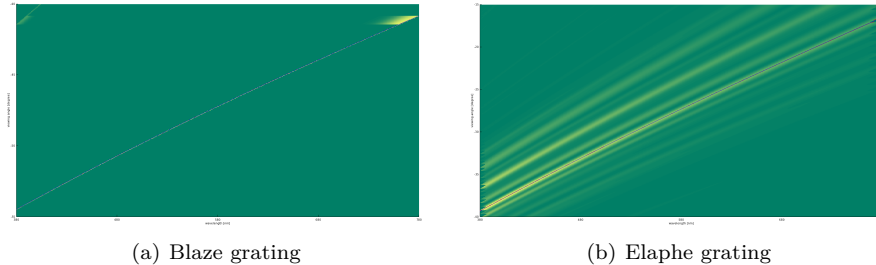


Figure 1.10: Reflectance obtained using $N_{min}N_{max}$ optimization approach

Last let us consider the evaluation graphs of the PQ approach ?? in figure 1.11. The PQ

approach assumes the given grating being periodically distributed on a shape's surface. For this approach we have plotted evaluation graphs of the Blaze- 1.11(a) and Elaphe grating 1.11(b). For both graphs their response curves have some similarities but also some differences compared to their corresponding grating equation curve. We could say that the response curve of the blaze grating is weakly oscillating around the grating equation curve (blue) but basically following it even there are some outliers. The response curve of the Elaphe grating is not following its corresponding first order grating equation curve rather another response curve for the PQ approach. This could be due to the assumption of the PQ approach that a given patch must be periodically distributed along the surface which is actually not that case. Nevertheless, the red curve fits one of the response curves.

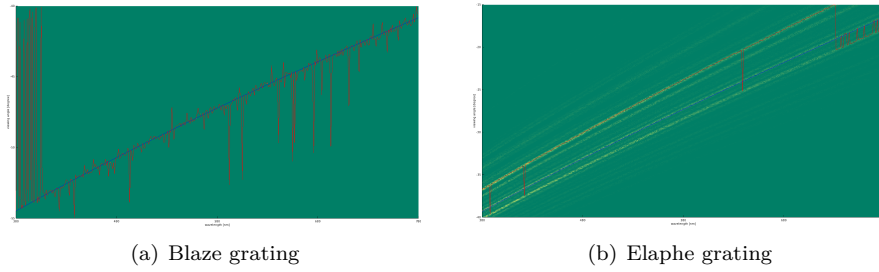


Figure 1.11: Reflectance obtained using PQ optimization approach

Chapter 2

Results

In this chapter we examine the rendered output results of our implementation of our BRDF models applied to different input patches such as Blaze grating or Elaphe ?? and Xenopeltis ?? snake nano-scaled surface sheds. We are discussing and comparing both, their BRDF maps 2.1 and the corresponding renderings on a snake geometry like shown in section 2.2 for various input parameters. Last we also show a real experimental image showing the effect of diffraction for similar parameters like we have.

2.1 BRDF maps

A BRDF map shows a shader's output for all possible viewing directions for a given, fixed, incident light direction. We assume that each viewing direction is expressed in spherical coordinates (See appendix ??) (θ_v, ϕ_v) and is represented in the map at point

$$(x, y) = (\sin(\theta_v)\cos(\phi_v), \sin(\theta_v)\sin(\phi_v)) \quad (2.1)$$

with its origin at the map-center. The light direction for normal incidence (θ_i, ϕ_i) has been fixed to $(0, 0)$ for our rendered results.

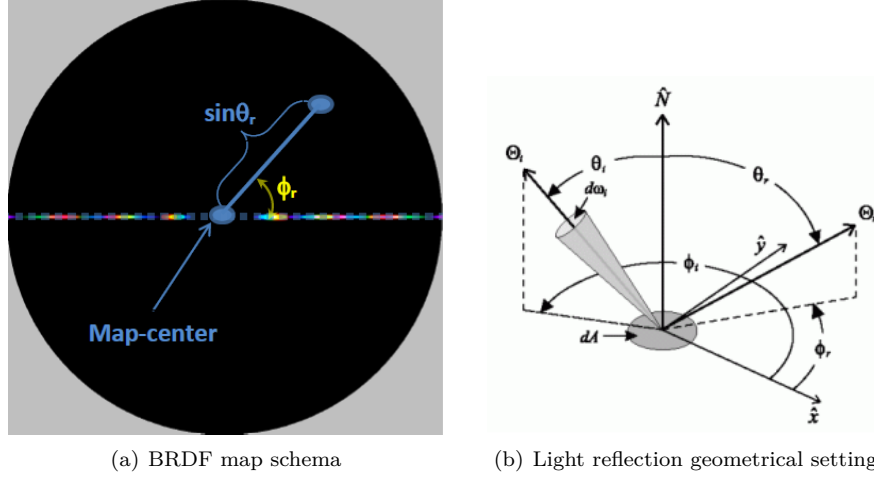


Figure 2.1: BRDF maps for different patches: $\Theta = (\theta_i, \phi_i)$ is the direction of light propagation

In this chapter we examine the rendered output resulting by the implementation of our BRDF models applied on different input patches 2.2 such as Blaze grating or Elaphe ?? and Xenopeltis ?? snake nano-scaled surface sheds. We going to discuss and compare both, their BRDF maps 2.1 and the corresponding renderings on a snake geometry 2.2 for various input parameters. Last we also show a real experimental image showing the effect of diffraction for similar parameters like we have. A BRDF map shows a shader's output for all possible viewing directions for a given, fixed, incident light direction. We assume that each viewing direction is in spherical coordinates form ?? (θ_v, ϕ_v) and is represented in the map at point $(x, y) = (\sin(\theta_v)\cos(\phi_v), \sin(\theta_v)\sin(\phi_v))$ with its origin at the map-center. The light direction for normal incidence (θ_i, ϕ_i) has been fixed to $(0, \pi)$ for our rendered results.

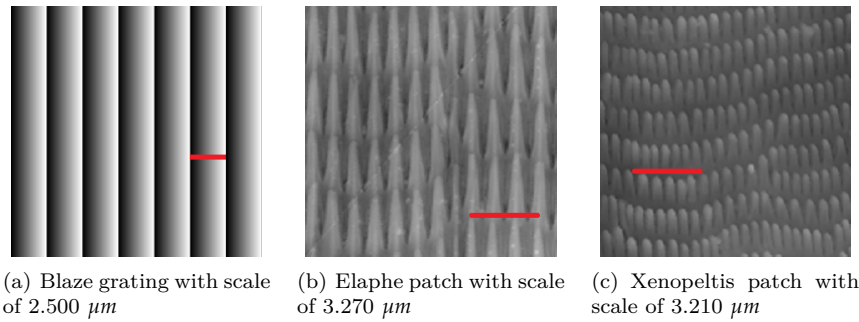


Figure 2.2: Cutouts of our nano-scaled surface gratings used for rendering within our shader with a scale indicator (red line) for each patch. Note that for rendering we use larger patches.

Figure 2.3 shows the BRDF maps of the full lambda space sampling approach ?? applied on different nanoscale surface gratings as shown in figure 2.2. In Subfigure 2.2(a) we see the BRDF map for the Blazed grating, showing high relative brightness for its first order diffraction which means that for the Blazed gratings most of the diffracted spectral energy lies in its first order. Note that for Blazed grating their first-order diffracted light returns along the same path as the incident light. Higher diffraction orders are still perceivable (second and third order diffraction)

but with a much lower relative brightness. The asymmetry of the pattern is due to the asymmetric geometry of the grating 2.2(a).

The finger-like structures contained in the Elaphe surface grating 2.2(b) are quite regularly aligned and hence diffraction occurs along the horizontal axis for the BRDF map as shown in figure 2.3(b). The reason for not seeing any strong diffraction color contribution along other directions in the BRDF map is due to the fact that these ‘nano-fingers’ overlap across layers and thus do not exhibit any definite periodicity along finger direction.

For Xenopeltis surface grating 2.2(c), we observe diffraction along many different, almost in vertical directions in the BRDF map 2.3(c) since the layers of the finger-like structures do not overlap and are shifted significantly along their length but still exhibit some local consistency. A similar argument holds true for diffraction across locally periodic finger patches with slightly different orientations.

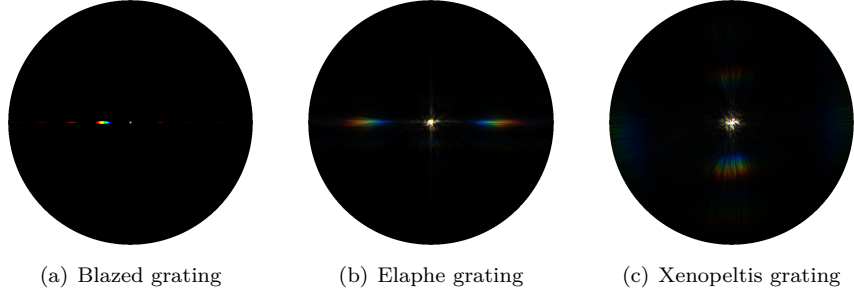


Figure 2.3: BRDF maps for different patches

TODO: CHANGE PQ, N MIN MAX IMAGE SINCE SINC INTERPOL IS MISSING Figure 2.4 shows a the BRDF maps of all our BRDF models applied on the Blaze grating. The most left figure 2.4(a) is showing the ground truth result for the Blazed grating used in order to compare with our other rendering approaches.

Figure 2.4(b) shows the BRDF map for the N_{min}, N_{max} approach which we assume to be close to the ground truth since its corresponding evaluation plots 1.10(a) already were closely matching. Nevertheless there is a small difference notable: since in the actual technical implementation of the N_{min}, N_{max} shading approach treats the center of the BRDF map as a separate case, i.e. everything around a small ϵ -circumference has white color assigned we note a white circular spot around the map center. Except this fact, the BRDF map resembles the ground truth.

Figure 2.4(c) shows the BRDF map for the PQ approach which relies on sinc-interpolation. As expected, after having considered the corresponding evaluation plots shown in figure 1.11(a), the PQ BRDF map and the ground truth are visual alike. Compared to the evaluation plots, the PQ BRDF maps even persuade more. One difference we notice is that the first order is a little spread. This effect is would be strengthened when using linear interpolation instead of sinc-interpolation.

Last, let us consider figure 2.4(d) which shows the BRDF map produced by using the implementation of Nvidia Gem’s implementation (ADD REFERENCE) of Stam’s BRDF model, when constraining the y-axis of the BRDF map. This model does not consider much more than the spacing d of a given grating. It also always produces highly symmetric results. It also does not render different orders of diffraction rather than the zero and first order.

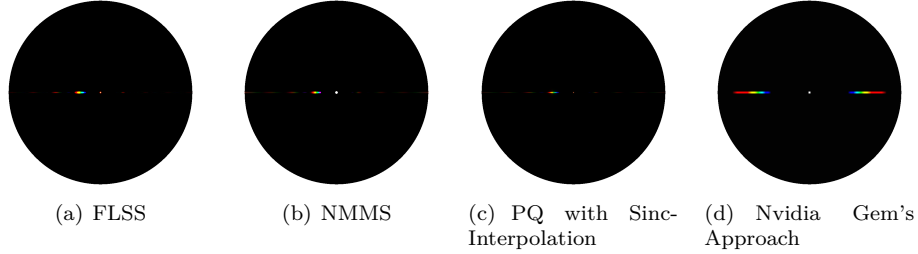


Figure 2.4: BRDF maps for Blazed grating comparing our different rendering approaches

Figure 2.5 and figure 2.6 show the BRDF maps for different wavelength step sizes used in the fragment shader for the full lambda space sampling approach applied on the Blaze grating and the Elpahne snake shed, respectively. Within our fragment shaders the most outer loop iterate over the range $[380nm, 780nm]$ for fixed step sizes λ_{step} which basically constitutes the integration over the wavelength spectrum. Therefore, having bigger step sizes implies having fewer step sizes which will fasten up the overall runtime of a shader but will also introduce artifacts and therefore lower the overall shading quality. For Elaphe surface grating, artifacts are perceptual arising when $\lambda_{step} \leq 10nm$. Results produced by using $5nm$ step sizes do not differ from those produced by using $\lambda_{step} = 1nm$ which allows us to set λ_{step} equal $5nm$. For a Blazed grating we may chose even bigger step sized without losing any rendering quality.

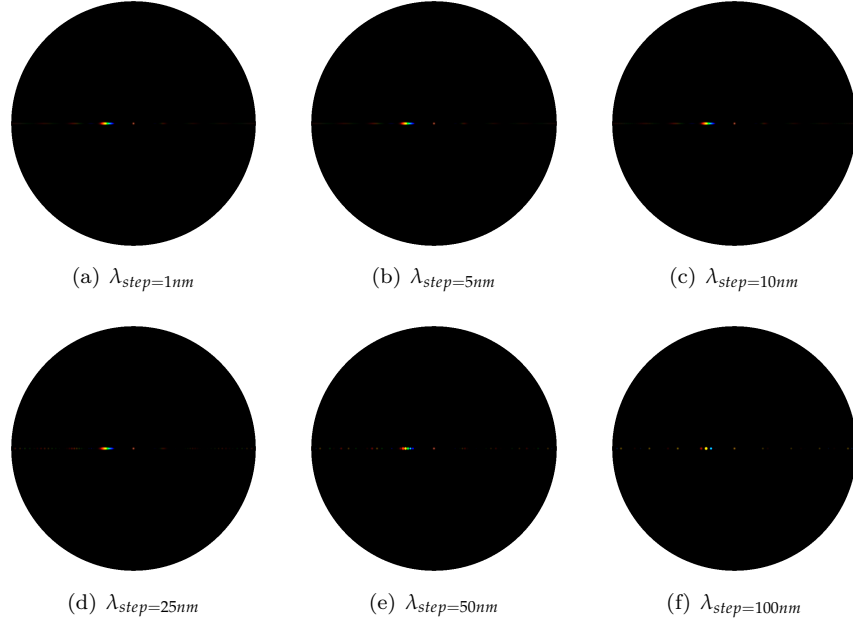
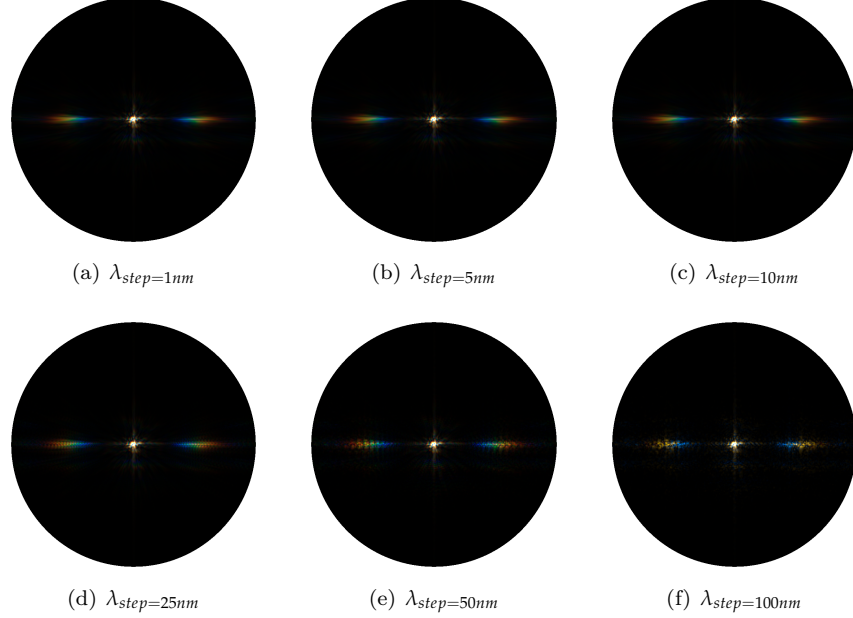


Figure 2.5: Blazed grating at $2.5\mu m$: Different λ step sizes

Figure 2.6: Elaphe grating at $65\mu m$: Different λ step sizes

The Figures 2.7, 2.9, 2.8 show a comparison of the BRDF maps produced by full lambda space sampling approach (on the left) and the PQ shading approach (on the right) applied on all our patches. For Blazed grating, as already mentioned, we notice that both approaches resemble each other. We also notice that for PQ map, the first order diffraction color contribution is spread. For Elaphe and Xenopeltis grating we notice similar shaped BRDF patterns, even when the angle of light varies, but nevertheless, they also contain some artifacts. This also holds true when we linearly interpolate instead relying on sinc-interpolation.

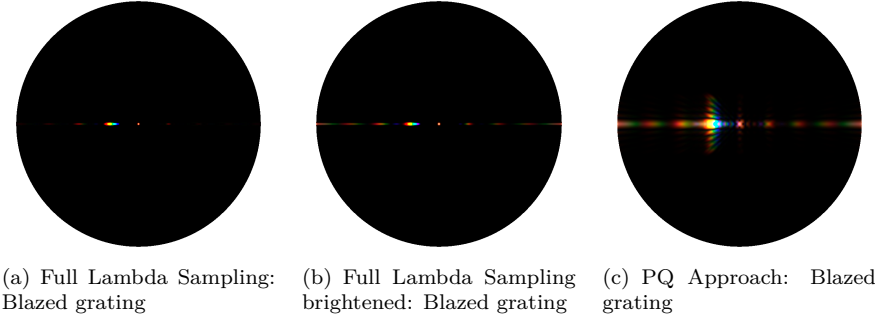


Figure 2.7: Blazed grating: PQ approach vs full lambda space sampling

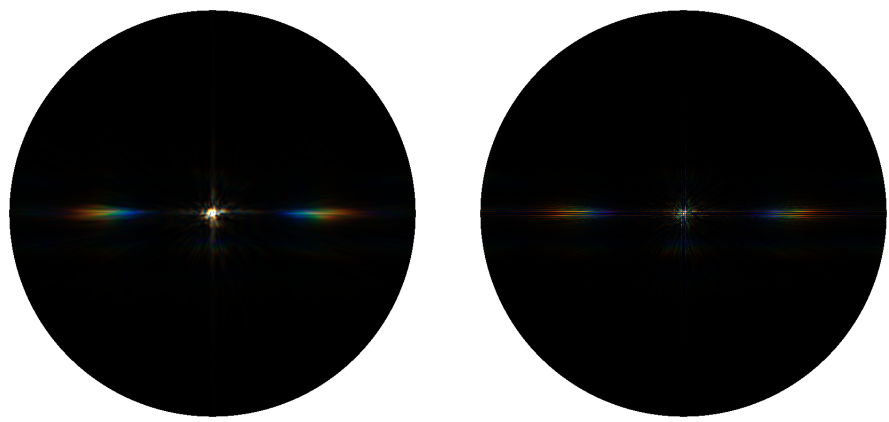


Figure 2.8: Elaphe grating: PQ approach vs full lambda space sampling

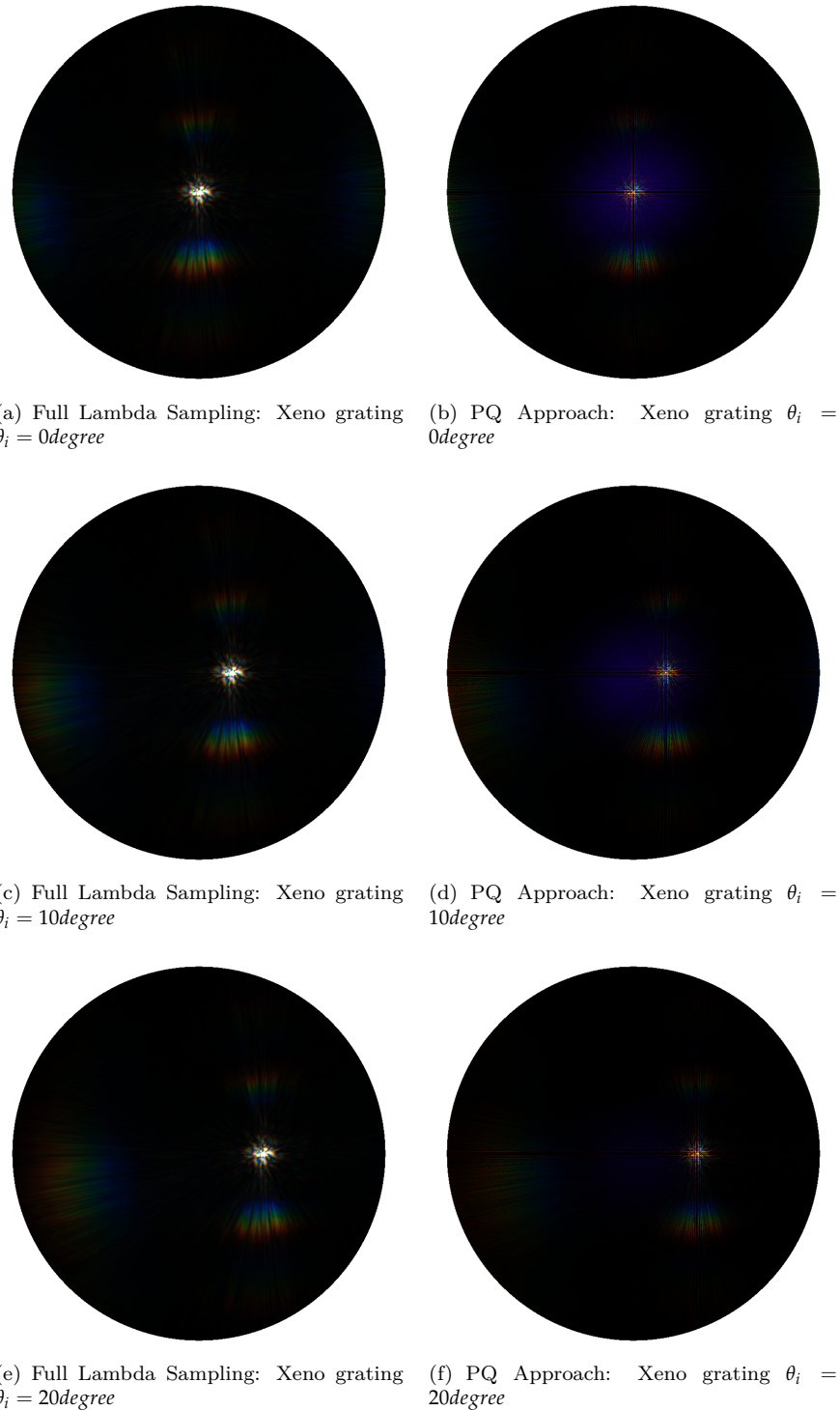


Figure 2.9: Xeno grating: PQ approach vs full lambda space sampling

Figure 2.10 shows BRDF map for the full lambda sampling approach applied on the Blazed grating, varying the value for the spacial variance σ_s . This is similar to consider the output of different coherence lengths for our incident light. The lower the coherence length, the fewer interacting grating periods produce produce blurred diffraction bands for different λ which overlap to produce poorly resolved colors.

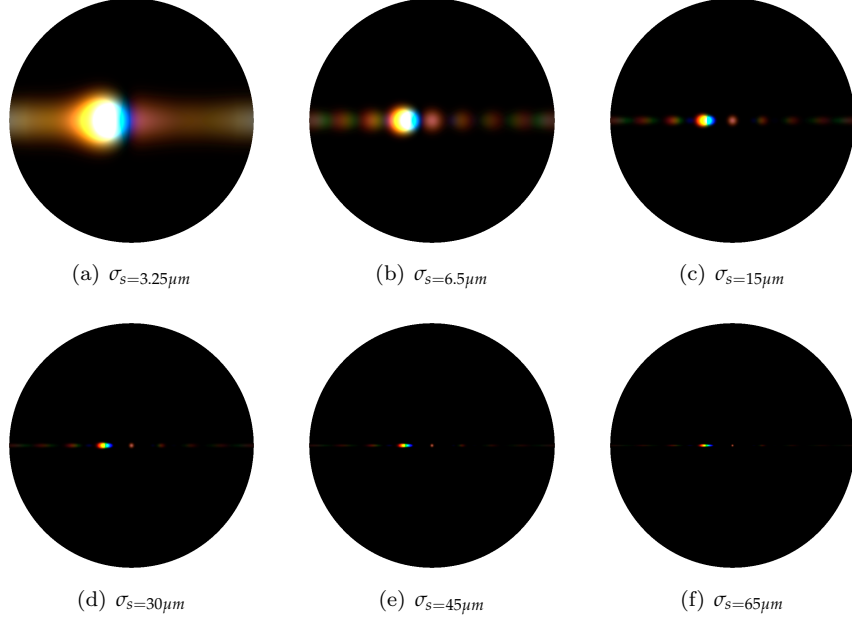


Figure 2.10: Blazed grating at $2.5\mu m$: Different σ_s sizes

The figures 2.11 and 2.12 show the BRDF maps of the full lambda space approach using different values for N used for the taylor series approximation used within our fragment shaders. For both input patches we clearly visually observe the convergence of the taylor series for higher values for N . We visually observe convergence of the Taylor series for all our from a certain value of N . In section ?? we already provided a proof for the convergence for a specific geometrical set up which could be applied easily to another setup. The higher the value of N the less the BRDF map changes. For the Blazed grating, we do not see much changing patterns for $N \geq 7$ and for the Elaphe surface grating $N \geq 9$. In general it is rather hard to say for what value of N we have visual convergence since in algorithm ?? we compute the inverse FFT of $power(1j * patchImg, t)$ which is equivalent to $iFFT(patchImg)^n \cdot i^n$. Since we multiply this by i^n there are four possible series where each converges within its own convergence radius.

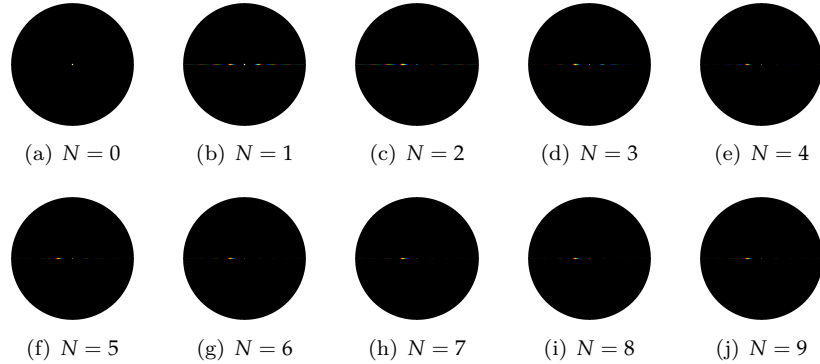
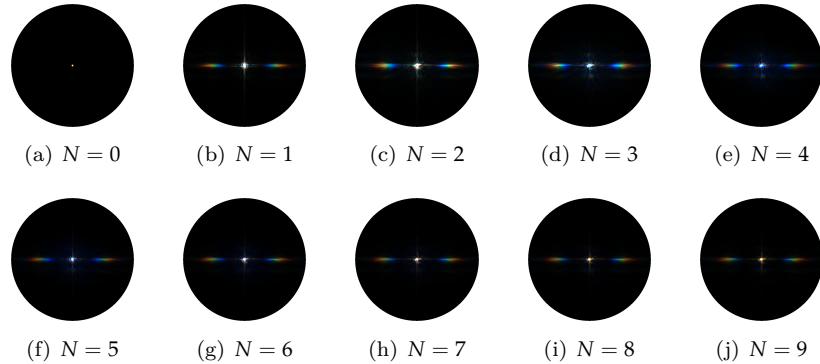
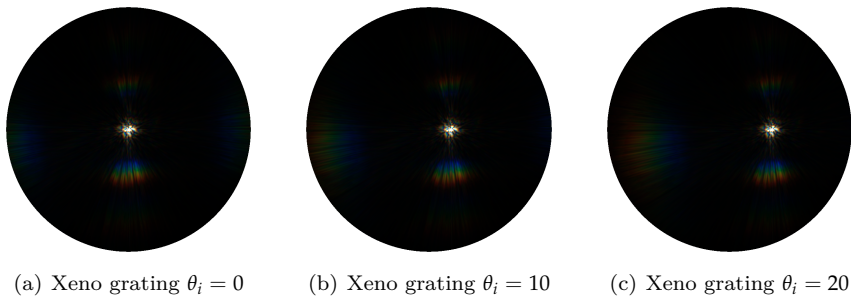
Figure 2.11: Blazed grating at $2.5\mu\text{m}$: N Taylor IterationsFigure 2.12: Elaphe grating at $65\mu\text{m}$: N Taylor Iterations

Figure 2.13 shows the BRDF maps of the full lambda shading approach applied on the Xenopeltis snake shed, using different θ_i incident angles. When slightly moving the incident angle θ_i , we can observe how the brdf map changes. For higher values of θ_i we start seeing diffraction color contribution on the right side of the BRDF map.

Figure 2.13: BRDF maps for Xeno grating: different θ_i angles

2.2 Snake surface geometries

In this section we are going to present our actual renderings simulating the effect of diffraction caused when a directional light source encounters different nano-scaled surfaces on a given curved snake mesh. We will see that diffraction colors change dramatically with changes in light direction, surface normals and viewing direction, which is typical for diffraction colors observed in nature. For rendering we are going to rely on our full wavelength space sampling approach. Unfortunately, this approach is rather slow and can barely be considered as being interactive performing. Nevertheless, we have introduced some optimizations in order to become interactive in rendering, such as the N_{min}, N_{max} approach, we are going to use this slow approach since this resembles the ground truth and therefore is the most accurate among all our presented approaches. As mentioned we are going to render diffraction on a given snake mesh. Note that we actually just have one particular mesh, for all our renderings we are going to use the same snake mesh which has been produced by 3d scanning an Elaphe snake species, consisting of 11696 vertices and 22950 faces. The reason for that is that it was hard to get a Xenopeltis snake ready for being 3d scanned. In addition, the micro-geometry is highly similar among snake species, it is the geometry of the nano-structures that are highly different among species and that cause the snake to be or not be iridescent. So, even Xenopeltis would not give you very different geometry than Elaphe. Table 2.1 lists the system specifications of the machine I used in order to produce the rendered images.

Processor	Intel i7 CPU 970 @ 3.20 GHz (12 CPUs)
Memory	12288 MB RAM
Graphics Card	GeForce GTX 770

Table 2.1: Hardware specifications of the machine which produced rendered results. Statistics are provided using the tool NVIDIA Geforce Experience.

Figure 2.14 shows renderings produced by the full lambda sampling approach applied on a snake shaped mesh for different given input patches. Due to the fact that a Blazed grating has its maximum intensity for a certain direction and the geometry of the snake mesh is curved which means non-flat, we can expect rather less diffraction color contribution like shown in figure 2.14(b). Differently for our other two gratings, Elaphe and Xenopeltis. For both renderings, we can see color contribution despite the effect of diffraction whereas we see much less colorful patterns for Elaphe 2.14(b) than for Xenopeltis 2.14(c). This also corresponds to the reality, considering the figure ?? as a reference. The nano-scaled surface structure of the species Elaphe as shown in figure 2.2(b) does not look that regular under the electron scanning microscope. This is why it is much less iridescent than the other species. Xeno has a brownish body with no pattern that makes the iridescence more spectacular than on Ellaphe.

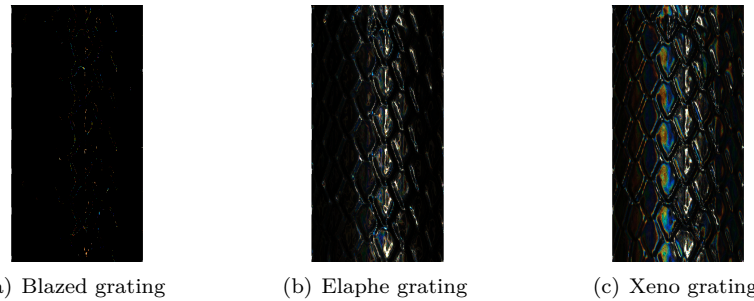


Figure 2.14: Diffraction of different snake skin gratings rendered on a snake geometry

Figure 2.15 contains a summary-collection of subfigures for rendering the effect of diffraction produced by the full lambda shading approach with all its required components, applied on our snake mesh, using the Elaphe nano-scaled surface structure. Subfigure 2.15(b) shows the final diffraction color-contribution result with texture-blending. We only see little diffraction color contribution in this subfigure which resembles quite well to the reality as shown in figure ???. In subfigure 2.15(d) we see the light cone in order to show the direction of the light source besides the rendered results. Subfigure 2.15(e) is a sample Fourier image of Elpahe's nanosclae surface structure 2.15(d).

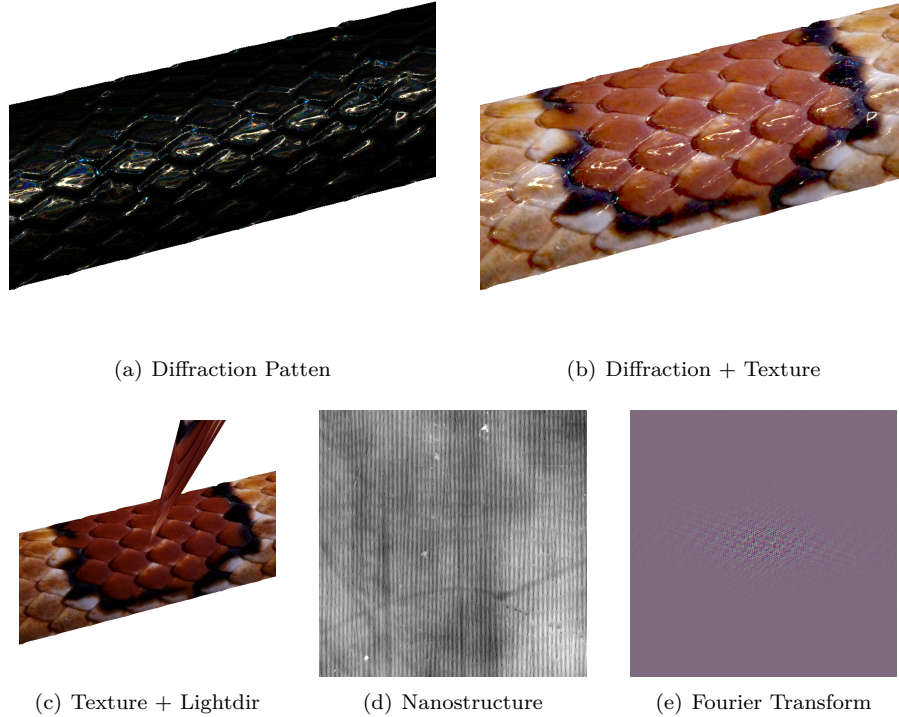


Figure 2.15: Diffraction for Elaphe snake skin

Like in the previous figure this figure 2.16 also shows a summary-collection of subfigures for the effect of diffraction with all its involved components but this time for the Xenopeltis snake surface. For texture blending we use the same texture like we used for Elaphe. For Xenopeltis see quite a lot color contribution due the phenomenon of diffraction like shown in figure 2.16(b). Comparing this to a real image ?? we notice much resemblance regarding the reflectance strength and colorful pattern.

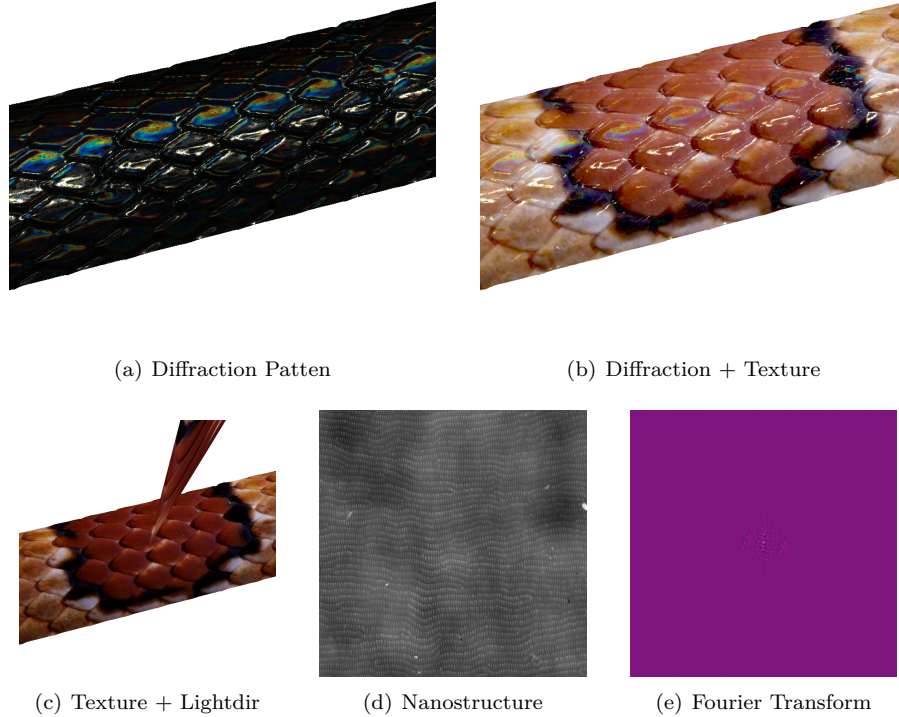


Figure 2.16: Diffraction for Xeno snake skin

Figure 2.17 shows the diffraction pattern of a Elaphe snake shed for different zoom levels for fixed incident light and viewing direction using the full lambda sampling approach. From those different close up perspectives it would appear the complexity of the colorful diffraction pattern.

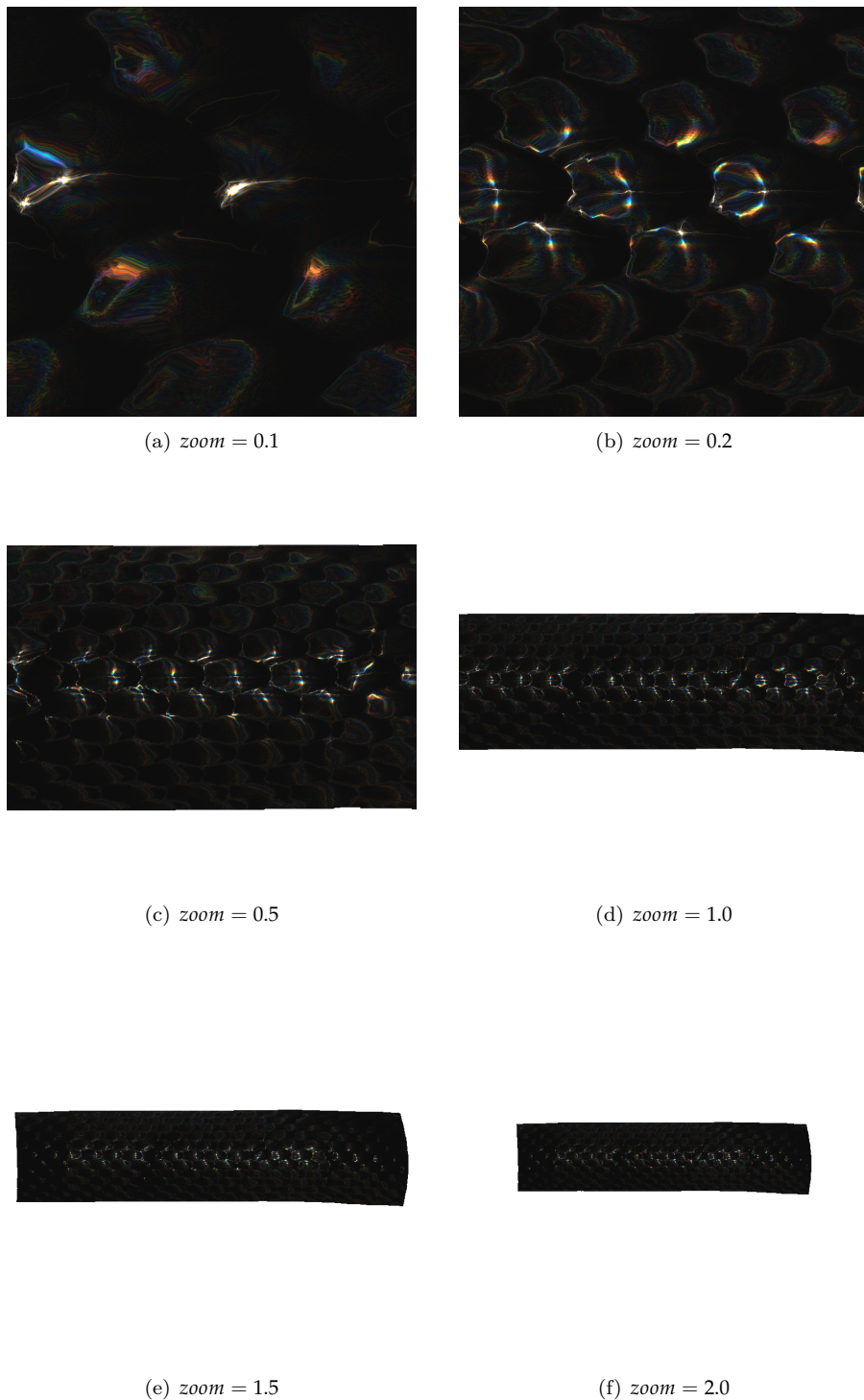


Figure 2.17: Diffraction on Elaphe snake skin grating: Different camera zoom levels

Figure 2.18 shows how the diffraction pattern changes when slightly moving the incident light direction. Which gives us an impression what kind of complex, perspective-dependent pattern the phenomenon of diffraction may cause.

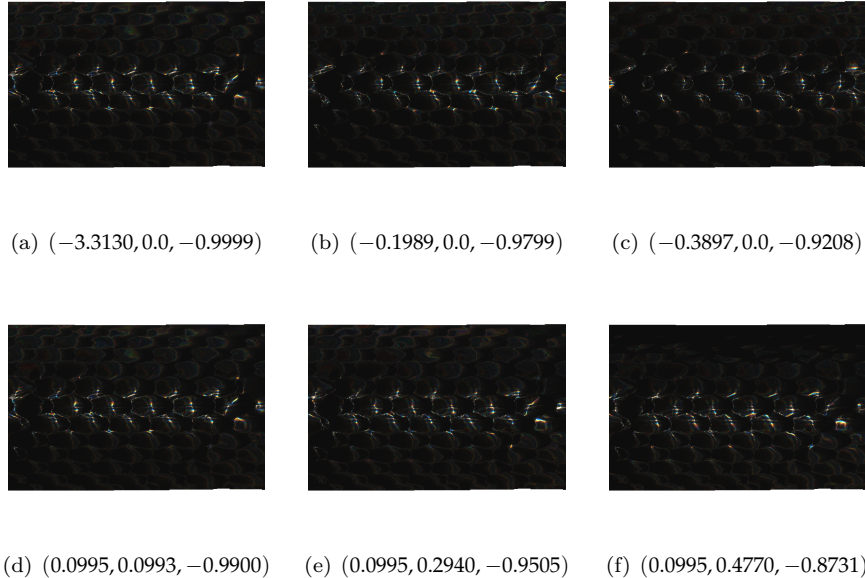


Figure 2.18: Diffraction on Elaphe snake skin grating: Different light directions

Figure 2.19 shows a photo of an experimental setup for demonstrating the effect of diffraction using a Elaphe snake grating. The exact parameters for the experimental setup are unknown. Nevertheless this image gives us an impression of how close our model is to the reality comparing it with our simulated results since we notice similar diffraction patterns for our simulated results using an Elaphe snake shed.

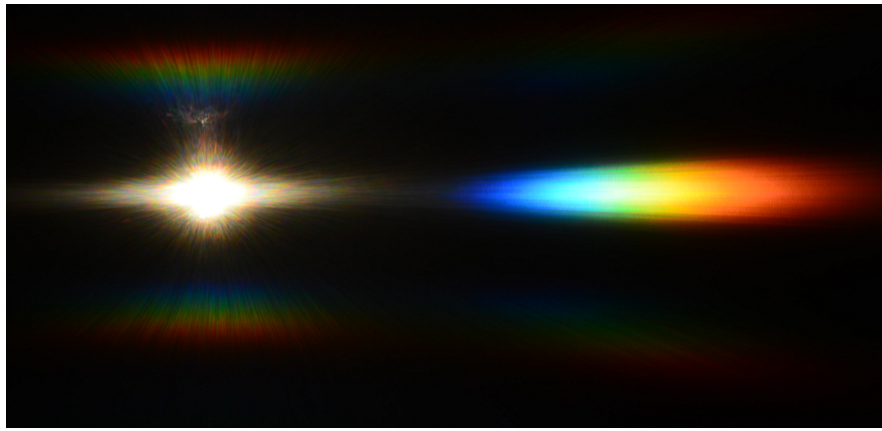


Figure 2.19: Diffraction Elaphe: experimental setup

List of Tables

1.1	Estimated Grating Spacings	10
2.1	Hardware Specifications	21

List of Figures

1.1	Spectrometer	2
1.2	Light directed to parallel to grating:	3
1.3	Diffraction Orders	4
1.4	Diffracted White Light	4
1.5	Intensity Plots for Different Number of Slits	5
1.6	Difference of diffraction pattern between a monochromatic (top) and a white (bottom) light spectra for different number of slits.	6
1.7	Experimental Setup	7
1.8	Reflective Grating	7
1.9	Reflectance obtained by using the shading approach described in algorithm ?? simulating a BRDF which models the effect of diffraction at different viewing angles over the spectrum of visible light.	9
1.10	Reflectance obtained using $N_{min}N_{max}$ optimization approach	10
1.11	Reflectance obtained using PQ optimization approach	11
2.1	BRDF Map	13
2.2	Our Gratings	13
2.3	BRDF Map FLSS of our Gratings	14
2.4	BRDF Map using our Approaches for Blazed Grating	15
2.5	BRDF Map varying step sizes FLSS Blazed Grating	15
2.6	BRDF Map varying step sizes FLSS Elaphe Grating	16
2.7	Blazed grating: PQ approach vs full lambda space sampling	16
2.8	Elaphe grating: PQ approach vs full lambda space sampling	17
2.9	Xeno grating: PQ approach vs full lambda space sampling	18
2.10	Blazed grating at $2.5\mu m$: Different σ_s sizes	19
2.11	Blazed grating at $2.5\mu m$: N Taylor Iterations	20
2.12	Elaphe grating at $65\mu m$: N Taylor Iterations	20
2.13	BRDF maps for Xeno grating: different θ_i angles	20
2.14	Diffraction of different snake skin gratings rendered on a snake geometry	22
2.15	Diffraction for Elaphe snake skin	23
2.16	Diffraction for Xeno snake skin	24
2.17	Diffraction on Elaphe snake skin grating: Different camera zoom levels	25
2.18	Diffraction on Elaphe snake skin grating: Different light directions	26
2.19	Diffraction Elaphe: experimental setup	26

List of Algorithms

1	Vertex diffraction shader	8
---	-------------------------------------	---

Bibliography

- [Bar07] BARTSCH, Hans-Jochen: *Taschenbuch Mathematischer Formeln*. 21th edition. HASNER, 2007. – ISBN 978–3–8348–1232–2
- [CT12] CUYPERS T., et a.: Reflectance Model for Diffraction. In: *ACM Trans. Graph.* 31, 5 (2012), September
- [DSD14] D. S. DHILLON, et a.: Interactive Diffraction from Biological Nanostructures. In: *EUROGRAPHICS 2014/ M. Paulin and C. Dachsba*cher (2014), January
- [For11] FORSTER, Otto: *Analysis 3*. 6th edition. VIEWEG+TEUBNER, 2011. – ISBN 978–3–8348–1232–2
- [I.N14] I. NEWTON: *Opticks, reprinted*. CreateSpace Independent Publishing Platform, 2014. – ISBN 978–1499151312
- [JG04] JUAN GUARDADO, NVIDIA: Simulating Diffraction. In: *GPU Gems* (2004). <https://developer.nvidia.com/content/gpu-gems-chapter-8-simulating-diffraction>
- [LM95] LEONARD MANDEL, Emil W.: *Optical Coherence and Quantum Optics*. Cambridge University Press, 1995. – ISBN 978–0521417112
- [MT10] MATIN T.R., et a.: Correlating Nanostructures with Function: Structrural Colors on the Wings of a Malaysian Bee. (2010), August
- [PAT09] PAUL A. TIPLER, Gene M.: *Physik für Wissenschaftler und Ingenieure*. 6th edition. Spektrum Verlag, 2009. – ISBN 978–3–8274–1945–3
- [PS09] P. SHIRLEY, S. M.: *Fundamentals of Computer Graphics*. 3rd edition. A K Peters, Ltd, 2009. – ISBN 978–1–56881–469–8
- [R.H12] R. HOOKE: *Micrographia, reprinted*. CreateSpace Independent Publishing Platform, 2012. – ISBN 978–1470079031
- [RW11] R. WRIGHT, et a.: *OpenGL SuperBible*. 5th edition. Addison-Wesley, 2011. – ISBN 978–0–32–171261–5
- [Sta99] STAM, J.: Diffraction Shaders. In: *SIGGRPAH 99 Conference Proceedings* (1999), August
- [T.Y07] T. YOUNG: *A course of lectures on natural philosophy and the mechanical arts Volume 1 and 2*. Johnson, 1807, 1807

Erklärung

gemäss Art. 28 Abs. 2 RSL 05

Name/Vorname:

Matrikelnummer:

Studiengang:

Bachelor

Master

Dissertation

Titel der Arbeit:

.....

.....

LeiterIn der Arbeit:

.....

Ich erkläre hiermit, dass ich diese Arbeit selbständig verfasst und keine anderen als die angegebenen Quellen benutzt habe. Alle Stellen, die wörtlich oder sinngemäss aus Quellen entnommen wurden, habe ich als solche gekennzeichnet. Mir ist bekannt, dass andernfalls der Senat gemäss Artikel 36 Absatz 1 Buchstabe o des Gesetztes vom 5. September 1996 über die Universität zum Entzug des auf Grund dieser Arbeit verliehenen Titels berechtigt ist.

.....
Ort/Datum

.....
Unterschrift